ADVANCED ENGINEERING *MATERIALS*

Optimization of Nanostructured Metals

SPM Patterning of Metallic Nano-Structures

Deformation of Bulk Metallic Glasses

Zeolites with Hierachical Porosity

WILEY-
VCH

DGM   SF2M   SVMT

COMMUNICATIONS

On the Impact of Macroscopic Phase Separation on Solidification Microstructures**

By *Menghuai Wu,* Andreas Ludwig, Mark Pelzer, Ulrich Postl*

By using the term "phase separation" we have a spatial separation due to the relative movement between different liquid and solid phases in mind. This relative movement might

[*] Dr. M. Wu, Prof. A. Ludwig
Simulation and Modeling of Metallurgical Processes
Dept. of Metallurgy, Uni. of Leoben
Franz-Josef-Str. 18, A – 8700 Leoben, Austria
Email: menghuai.wu@notes.unileoben.ac.at
Dr. M. Pelzer, Dipl. Ing. U. Postl
Fluent Deutschland GmbH
Birkenweg 149, D – 64295 Darmstadt, Germany

be caused by one of the following mechanisms: thermosolutal convection, grain sedimentation and sedimentation-induced melt convection, feeding flow through stationary (columnar) or packed (equiaxed) grains, or capillary force driven (Marangoni) flow. Recently the authors have developed a multiphase modeling technique in order to study solidification processes governed by the above given macroscopic phase separation phenomena.[1-5] This paper will report three of the latest modeling achievements: (1) macrosegregation formation caused by grain sedimentation and melt convection in an Al–4 wt.% Cu casting; (2) gravity- and Marangoni-induced droplet motion during directional solidification of an Al–10 wt.% Bi hypermonotectic alloy; and (3) mixed columnar-equiaxed solidification in a binary Fe-0.34 wt.% C "steel" ingot. The presented results demonstrate the role of phase separation phenomena in solidification, and give an idea about the different mechanisms which govern the formation of microstructure and macrosegregations.

The multiphase modeling technique presented in this paper considered the following relative movements: (1) movement between a liquid and a solid, e.g. sedimentation of the equiaxed globular grains or interdendritic melt flow (Fig. 1(a-b)); (2) movement between two liquids, e.g. two immiscible liquid phases during hypermonotectic solidification (Fig. 1(c)); and (3) movement between two solids, e.g. free moving globular grains with respect to stationary columnar dendrites (Fig. 1(a)). Although gas might also appear during solidification (porosity), it is not explicitly modeled at present.

Only in recent years has it become possible to model these multiphase relative movements which appear during solidification. The first attempt based on the volume-averaging approach was established by Beckermann's group.[9-13] Their model was further modified by the authors and extended to solidification problems considering the above mentioned different categories of relative movements.[1-5]

The considered phases are treated as interpenetrating continua with a certain volume fraction f_q subject to

$$\sum_{q=1}^{\tilde{n}} f_q = 1$$

Here, q is the phase index and $\tilde{n}$ the number of phases. The phases are allowed to move relatively to each other according to mass and momentum conservation equations. Decomposition and solidification are considered according to appropriate thermodynamic and kinetic transition laws. Details on the model assumptions are described in the original publications.[1-5] The conservation equations are summarized here in short:

Mass:

$$\frac{\partial}{\partial t} f_q \rho_q + \nabla \cdot f_q \rho_q \vec{u}_q = \sum_{p=1(\neq q)}^{\tilde{n}} \dot{m}_{pq} \tag{1}$$
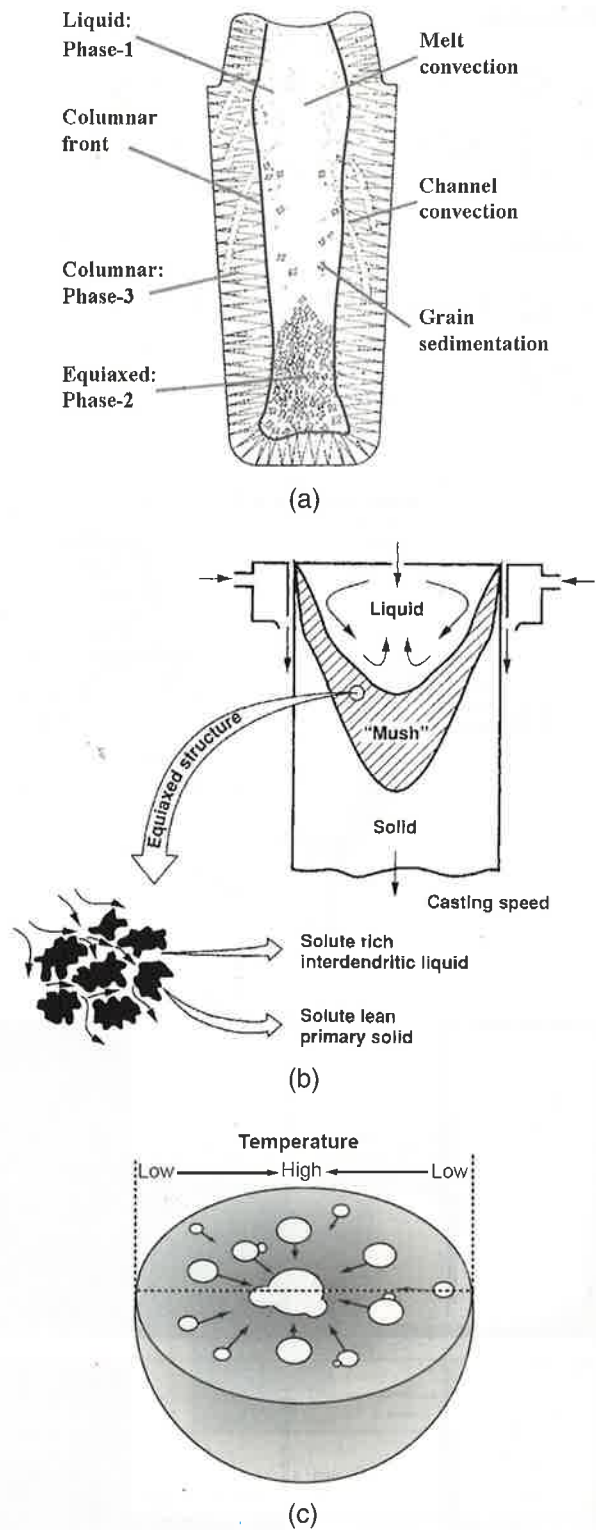

(a)

(b)

(c)

Fig. 1. Examples of phase separation phenomena during solidification. a) Grain sedimentation and melt convection in steel ingot casting [6]. b) Melt convection and interdendritic flow in continuous casting [7]. c) Droplet motion of secondary liquid phase by Marangoni effect, and evolution of the egg-type structure in an immiscible alloy powder [8].

Momentum:

$$\frac{\partial}{\partial t}\left(f_q\rho_q\vec{u}_q\right) + \nabla\cdot\left(f_q\rho_q\vec{u}_q\otimes\vec{u}_q\right) = -f_q\nabla P + \nabla\cdot\bar{\bar{\tau}}_q +$$
$$f_q\rho_q\vec{g} + \sum_{p=1(\neq q)}^{\tilde{n}} K_{pq}\left(\vec{u}_p - \vec{u}_q\right) + \sum_{p=1(\neq q)}^{\tilde{n}} \vec{u}_{pq}^{*}\cdot\dot{m}_{pq} + \vec{F}_q \quad (2)$$

Enthalpy:

$$\frac{\partial}{\partial t}\left(f_q\rho_q h_q\right) + \nabla\cdot\left(f_q\vec{u}_q h_q\right) = \nabla\cdot\left(f_q k_q\nabla\cdot T_q\right) +$$
$$\sum_{p=1(\neq q)}^{\tilde{n}} H_{pq}\left(T_p - T_q\right) + \sum_{p=1(\neq q)}^{\tilde{n}} h_{pq}^{*}\cdot\dot{m}_{pq} \quad (3)$$

Species:

$$\frac{\partial}{\partial t}\left(f_q\rho_q c_q^i\right) + \nabla\cdot\left(f_q\rho_q\vec{u}_q c_q^i\right) = \nabla\cdot\left(f_q\rho_q D_q^i\nabla c_q^i\right) +$$
$$\sum_{p=1(\neq q)}^{\tilde{n}} c_{pq}^{i*}\cdot\dot{m}_{pq} \quad (4)$$

Number density of grains/droplets:

$$\frac{\partial}{\partial t}n + \nabla\cdot\left(\vec{u}_q\cdot n\right) = \dot{n} \quad (5)$$

By solving these equations, the dependent quantities are obtained for all phases: volume fraction f_q, velocity $\vec{u}_q$, enthalpy

(a)

Casting: Al-4wt.%Cu
$T_0 = 925\,K$
$c_0 = 0.04$
$g = -9.81\,m\,s^{-2}$

$T_{mold} = 290\,K$
$H = 750\,W\,m^{-2}\cdot K^{-1}$

(b)

(c)

$t = 6\,s$
$\bar{u}_{s,max} = 53\ mm/s$
$f_s: 0 \sim 0.37$
$c_{mix}: 0.0315 \sim 0.0485$

$t = 12\,s$
$\bar{u}_{s,max} = 47\ mm/s$
$f_s: 0 \sim 0.62$
$c_{mix}: 0.0315 \sim 0.0485$

$t = 18\,s$
$\bar{u}_{s,max} = 53\ mm/s$
$f_s: 0 \sim 0.75$
$c_{mix}: 0.0315 \sim 0.0485$

$t = 105\,s$
$\bar{u}_{s,max} = 0.2\ mm/s$
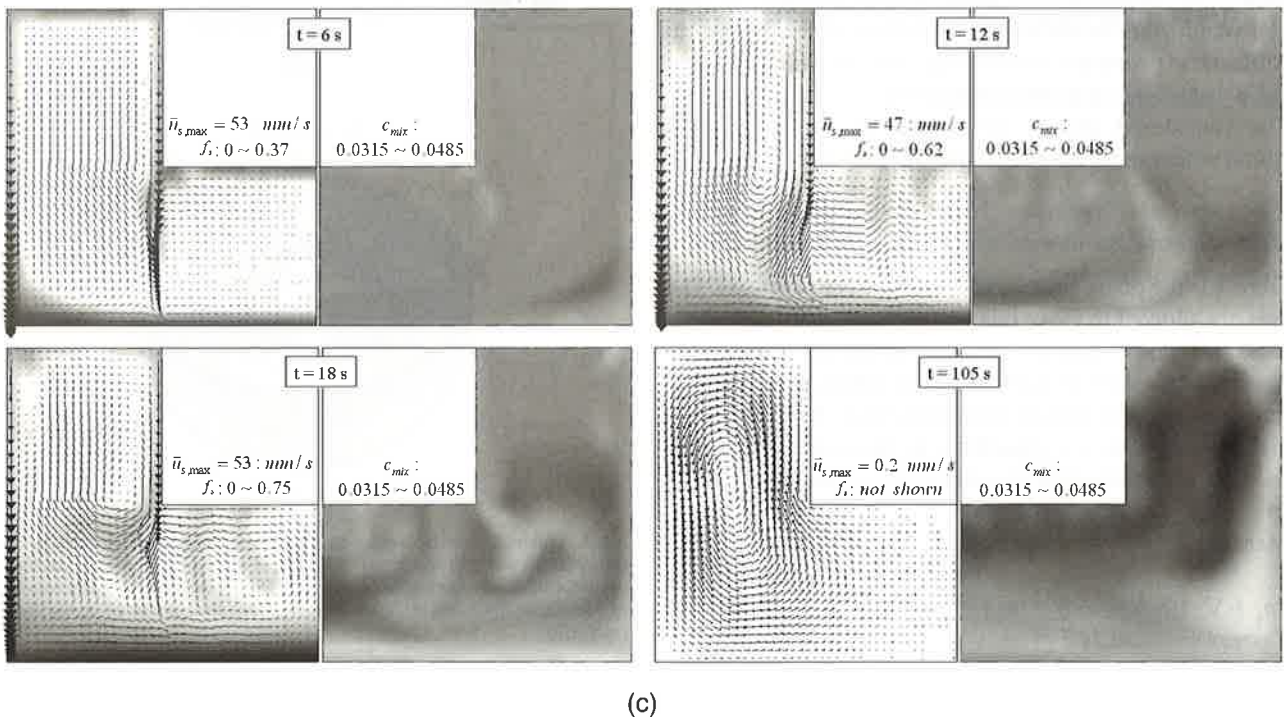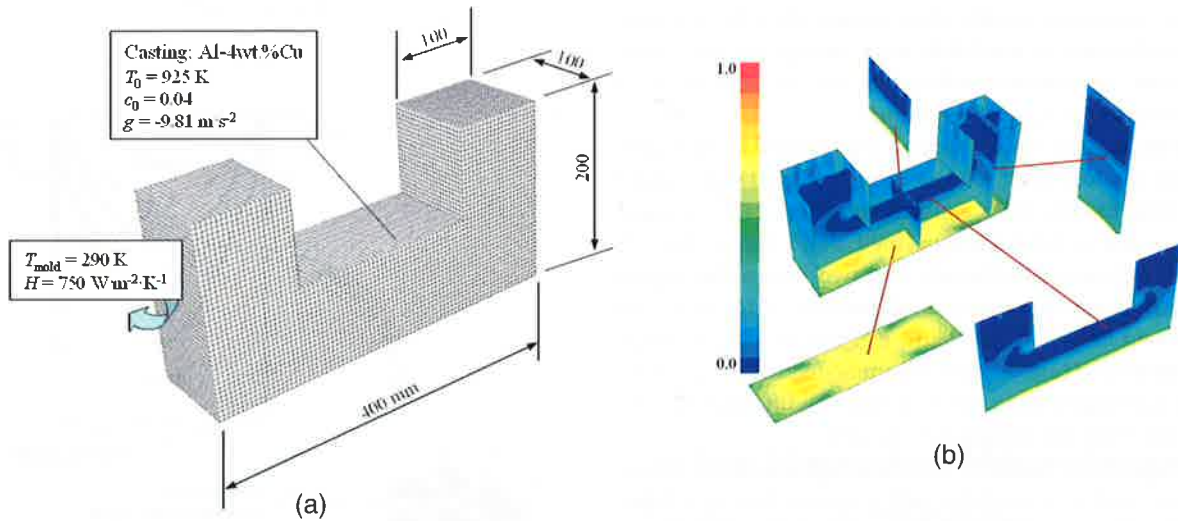$f_s: not\ shown$
$c_{mix}: 0.0315 \sim 0.0485$

Fig. 2. Solidification and macrosegregation formation of an Al-4 wt.%Cu die casting: (a) U-shape die casting configuration, (b) solid fraction at $t = 10$ s in 3D and (c) grain sedimentation, solidification and the resulting formation of macrosegregations in the middle section of (a).

h_q (i.e. temperature T_q), and concentration of the i-species c^i_q. In addition, the number density of secondary objects (grains or droplets) n is calculated by the conservation equation, Eq. 5. The pressure field P is shared by all phases. With some auxiliary relations, additional quantities such as the size of the secondary objects, d_e, or the mixture concentration, c_{mix}, are calculated, like e.g.

$$d_e = \sqrt[3]{6f_e/(\pi n)} \qquad (6)$$

and

$$c^i_{mix} = \sum_{p=1}^{\tilde{n}} c^i_p f_p \rho_p \Bigg/ \sum_{p=1}^{\tilde{n}} f_p \rho_p \qquad (7)$$

To investigate the formation of macro-segregation in the presence of grain sedimentation a U-shaped Al-Cu die casting was simulated (Fig. 2). In this case, only two phases were considered: melt and globular equiaxed grains. The equiaxed grains are allowed to nucleate near the wall and, less pronounced, in the bulk melt. They are free to move as long as their volume fraction is below the so-called "packing limit" (f_s^c=0.637). The casting is assumed to be filled instantaneously and solidified in a closed die of 290 K. In order to enhance the cooling and thus to stimulate grain nucleation and subsequently sedimentation, a steel chill is intentionally placed in the upper middle region of the die. All thermal-physical material properties and the process parameters used for the simulation can be found in reference.[14]

Grains which nucleate near the steel chill and also at the sidewalls sink downwards (see Fig. 2 (b,c)). The sinking grains lead to an accumulation of the solid phase in the bottom region of the casting. The grains stop moving and finally settle at the latest when the local fraction of solid exceeds the packing limit. The grain settlement is the main reason for the negative segregation at the bottom of the casting. With proceeding solidification, this negative segregation zone becomes wider and wider. The strongest negative segregations are found in the lower cor-
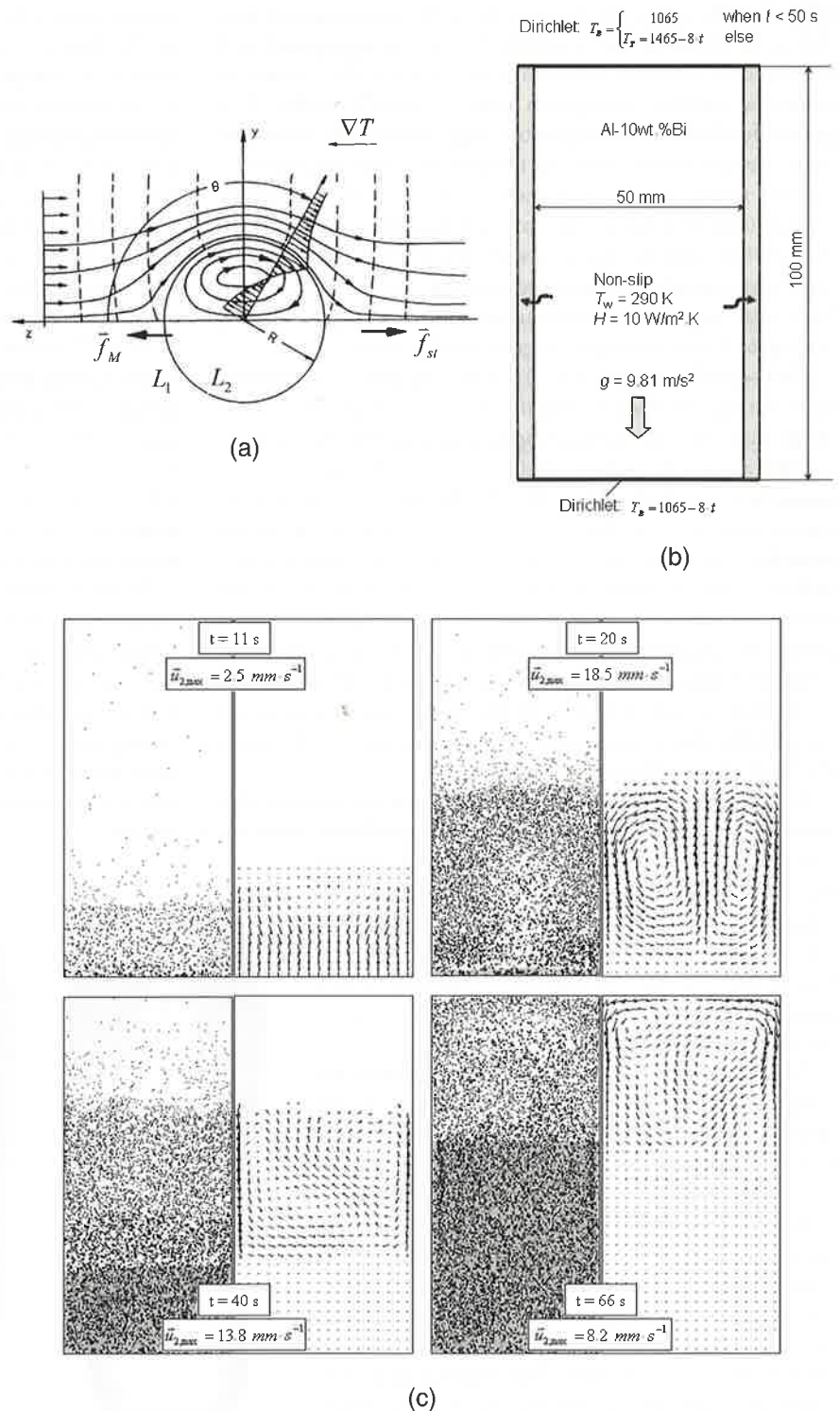

(a)

(b)

(c)

Fig. 3. (a) Temperature-dependent thermo-capillary force drives the convection in/around the L_2 droplet. Marangoni force $\vec{f}_M$ drives the droplet to move in ∇T direction, and Stokes force $\vec{f}_{st}$ points to the reverse direction (b) Scheme of the simulated case (c) Formation of L_2 (Bi) droplets during directional solidification of hypermonotectic Al –10 wt.% Bi. Both the droplet density and the diameter of the droplets, shown in left hand side of each figure, are reduced and enlarged by corresponding factors so that the droplet distribution can be seen with the naked eye. The L_2 velocity fields, shown on the right-hand side of each figure, are continuously scaled starting from zero to the maximum value. The gray region indicates the solidified monotectic matrix.

ners near the sidewalls because there the grains accumulate and settle the most. As the residual positively segregated melt is diverged from the sedimentation zone by the settling of grains, a positive segregation zone is formed nearby. It is generally observed that a positive segregation zone exists just near a sedimentation zone. As this positive segregated zone is located within the melt at the boundary of the two-phase regions (mush), it is not stationary and may move with the melt flow. While solidification proceeds, the positively segregated melt areas move towards and accumulate gradually in the last-to-solidify region. This accumulation forms a large positively segregated zone at the late stage of solidification.

The second example (Fig. 3) shows the phase decomposition during directional solidification of a hypermonotectic Al-Bi alloy. At least 4 phases appear during hypermonotectic solidification: the parent melt ($L = L_1$), the decomposed secondary liquid phase L_2 (here Bi), the solidified monotectic matrix and the solidified secondary phase. The recent model considers the two liquids as individual movable phases. Solidification (monotectic reaction) is approximated in the somewhat classical way, by varying the thermo-physical properties accordingly. Thus, the viscosity of phase L_1 is enlarged while approaching the monotectic temperature. The L_2 droplets are entrapped by the the monotectic reaction front by applying also a corresponding viscosity increase. Of course, the heats of transitions are accounted for.

For hypermonotectic alloys, there are two mechanisms that drive the motion of the L_2 droplets: gravity-induced sedimentation and Marangoni force (Fig. 3(a)). In the following, we outline the simulation results gained for a directional solidification process of an Al-Bi alloy. The configuration of the simulated case is shown in Figure 3(b). Again, for the used thermo-physical material data and process parameters we refer to the original paper.[15]

Nucleation of L_2 (Bi) droplets starts as soon as the temperature drops below the binodal. Due to the applied cooling conditions, this first happens at the bottom area of the sample casting, seeing the result at 11 s. As the droplets form, they start to submerge and sediment towards the bottom. While the Bi-droplets grow and sink, further nucleation leads to a continuous creation of new Bi-droplets above the already existing ones. The collective downwards movement of droplets has to be compensated by an upwards movement of parent melt. This relative motion is inherently unstable, as in the classical Rayleigh-Bénard problem. As the downwards movement of droplets accelerates, the rising parent melt creates an upwards jet in the middle of the casting, which can be seen at Figure 3 (c) at $t = 20$ s. By this upwards jet of parent melt, some Bi droplets are carried from the bottom region into upper regions. However, due to their weight they tent to submerge and also calm down the parent melt again through the active

momentum exchange. In the meantime, the continuous cooling at the bottom causes the parent melt to solidify at the monotectic temperature and so freeze-in the Bi-droplets. This is visualised by the gray area which propagate from the bottom upwards, starting at $t = 20$ s. Note that the solidification front is not perfectly flat – a consequence of the convection-induced perturbations of isotherms. The final solidification result shows the depletion of the L_2 phase in upper region (0.966 vol.%) and an enrichment of L_2 in the middle bottom region (12.5 vol.%). Qualitatively, the above simulation results agree with experiments preformed by Alkemper and Ratke on a chilled cast Al-Bi alloys[16] and those by Fujii et al on an Al-Pb-Bi ingot casting under normal terrestrial condition:[17] depletion of Bi phase at the top of the sample and enrichment of Bi phase at the bottom. Quantitatively, the Alkemper and Ratke's experiments with 9.0 ~ 11.0 wt.% Bi alloys show about 1.5 vol.% at the top and 9.5 vol.% at the bottom. Considering the small geometrical differences and that the casting conditions are simplified in the recent numerical model, the agreement is quite satisfactory.

Figure 4 shows the predicted macrosegregation in a binary "steel" ingot (Fe-0.34 wt.%C) where mixed columnar-equiaxed solidification occur. Three phases appear in this case: melt, globular equiaxed grains, and the stationary columnar dendrites. Considering the high computation cost, a reduced casting size ($\varnothing$ 66 × 170 mm^2) is simulated. The casting is assumed to be filled instantaneously and starts to solidify from an initial temperature of 1785 K. The mold and surrounding air remain at 300 K. The heat transfer coefficient between casting
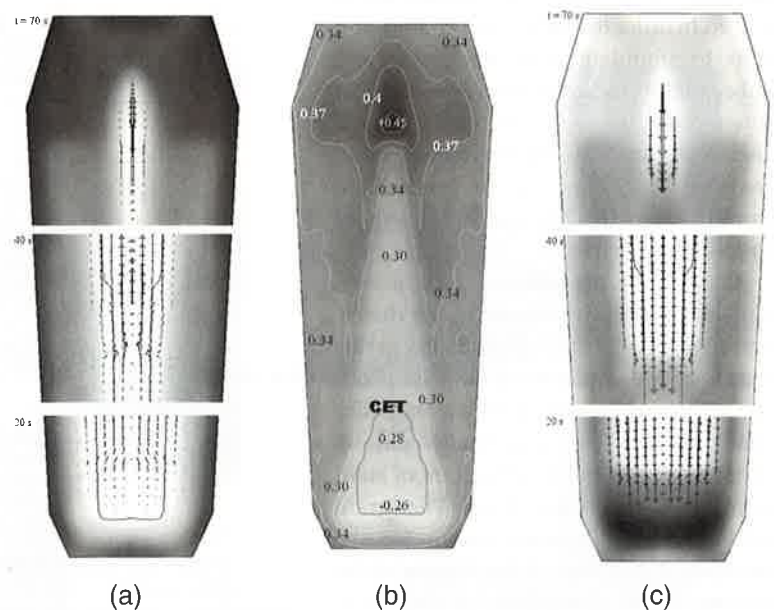

Fig. 4. Predicted solidification and macrosegregation in a binary "steel" ingot (Fe −0.34 wt.% C). c_{mix} is shown with both isolines and gray scale: light for negative segregation and dark for positive segregation. The values accompanying c_{mix} isolines are in unit of percentage. The CET (black line) is also drawn together with c_{mix}. In order to illustrate the formation of macrosegregations, the phase distribution fields f_e and f_c and the velocity fields $\vec{u}_l$ and $\vec{u}_e$ in three different sections (bottom, middle, top) corresponding to 3 different moments (20, 40, 70 s) are shown. The f_c and f_e are shown with 60 gray levels from minimum (0) to maximum (0.99). The columnar tip front (solid line) overlaps the quantities f_c and f_e. a) $f_c + \vec{u}_l$ at different time. b) c_{mix} c) $f_e + \vec{u}_e$ at different time.

and mold/air was assumed to be 700 Wm^{-2}K^{-1}, and 100 Wm^{-2}K^{-1} at top boundary. The material properties used and other modeling details are described elsewhere.[5]

The predicted solidification sequence including the sedimentation of the equiaxed grains and the evolution of negative and positive segregated regions (see Fig. 4) agrees well with the classical explanation of steel ingot solidification, which was summarized by Campbell[6] and is schematically shown in Figure 1(a). The columnar dendrites grow from the mold wall and the columnar tip front moves inwards. The equiaxed grains nucleate near the mold walls and in the bulk melt. The columnar dendrites are stationary, whereas the equiaxed grains sink and settle in base region of the ingot. The heap of such grains at the base of the ingot has a characteristic cone-shape. Two symmetrical melt convection vortices in the ingot are induced by both thermal-solutal effects and the drag of sinking grains. The grain sedimentation and melt convection influence the macroscopic solidification sequence and thus, the final phase distribution: more equiaxed grains will be found at bottom and base region and larger columnar areas in the upper part of the ingot.

As the columnar tip front is explicitly tracked in the model, the simulation shows that the columnar tip fronts from both sides tends to meet in the center part of the casting center. However, in the lower part of the casting the huge amount of equiaxed grains stops the propagation of the columnar tip front. Its final position indicates the so-called columnar to equiaxed transition i.e. CET. The CET separates areas where only equiaxed grains appear with those where both columnar dendrites and equiaxed grains might be found in common.

From the simulation results it becomes obvious that the main mechanism for the cone-shaped negative segregation in the base region is grain sedimentation. As the settling grains are poor in solute element, their pile-up induces negative segregation. A further contributing factor to the amount of negative segregation arises from the flow divergence of the residual liquid through this zone at a late solidification stage. These modeling results seem to reproduce the explanation, which was given by Campbell[6] based on the understanding of the classical experiments. The positive segregation at the top region of the ingot can be explained by the convection of the segregated melt in the bulk region (Fig. 4(a)). This kind of positive segregation coincides with the early experimental results of Nakagawa et al.[6,18] Finally, it must be mentioned that channel segregations, which are frequently found in steel ingots, are not predicted with the recent model. The reason for this is that melting was not taken into account in this simulation and that the used numerical grid is too coarse.

With the presented results, macroscopic phase separations governing the formation of microstructure and of macrosegregations are demonstrated. Actually, macrosegregations are caused by any relative movement between liquid and solid and the macrostructural phase distribution depends strongly on the phase transport mechanism acting. The presented multiphase modeling technique allows a deeper insight to be gained in

several relevant process details. However, there are still some refinements to the model necessary in order to apply such an approach to real industry castings.

[1] A. Ludwig, M. Wu, *Metall. Mater. Trans. A* **2002**, *33*, 3673.

[2] M. Wu, A. Ludwig, A. Bührig-Polaczek, M. Fehlbier, P. R. Sahm, *Int. J. Heat Mass Transfer* **2003**, *46*, 2819.

[3] M. Wu, A. Ludwig, L. Ratke, *Metall. Mater. Trans. A* **2003**, *34*, 3009.

[4] M. Wu, A. Ludwig, L. Ratke, *Modell. Mat. Sci. Eng.* **2003**, *11*, 755.

[5] M. Wu, A. Ludwig, *Metall. Mater. Trans. A* **2005**, (submitted).

[6] J. Campbell, *Castings*, Butterworth-Heinemann, Oxford **1991**.

[7] T. L. Finn, M. G. Chu, W. D. Bennon, *Mico/Macro Scale Phenomena in Solidification, ASME,* **1992**, *AMD-139*, 17.

[8] C. P. Wang, X. J. Liu, I. Ohnuma, R. Kainuma, K. Ishida, *Science* **2002**, *297*, 990.

[9] C. Beckermann, R. Viskanta, *Appl. Mech. Rev.* **1993**, *46*, 1.

[10] J. Ni, C. Beckermann, *Metall. Trans. B* **1991**, *22*, 349.

[11] C. Y. Wang, C. Beckermann, *Metall. Mater. Trans. A* **1996**, *27*, 2754.

[12] C. Beckermann, *JOM* **1997**, *49*, 13.

[13] C. Beckermann, *Intern. Mater. Rev.* **2002**, *47*, 243.

[14] M. Wu, A. Ludwig, J. Luo, *Mater. Sci. Forum* **2005**, *475–479*, 2725.

[15] A. Ludwig, M. Wu, M. Abondano, L. Ratke, *Mater. Sci. Forum* **2005**, (in press).

[16] J. Alkemper, L. Ratke, *Metall. Z.* **1994**, *85*, 365.

[17] H. Fujii, T. Kimura, H. Kitaguchi, H. Kumakura, K. Togano, *J. Mater. Sci.* **1995**, *30*, 3429.

[18] Y. Nakagawa, A. Momose, *Tetsu-to-Hagane* **1967**, *53*, 1477.